Hindawi
Journal of Nanomaterials
Volume 2019, Article ID 2840517, 10 pages
https://doi.org/10.1155/2019/2840517

Research Article

Melanin-Mediated Synthesis of Copper Oxide Nanoparticles and Preparation of Functional Agar/CuO NP Nanocomposite Films

Swarup Roy and Jong-Whan Rhim

Center for Humanities and Sciences, Bio-Nanocomposite Research Center, Department of Food and Nutrition, Kyung Hee University, 26 Kyungheedae-ro, Dongdaemun-gu, Seoul 02447, Republic of Korea

Correspondence should be addressed to Jong-Whan Rhim; jwrhim@khu.ac.kr

Received 10 October 2018; Accepted 17 December 2018; Published 6 February 2019

Academic Editor: Ovidiu Ersen

Copper oxide nanoparticles (CuO NP) were prepared using melanin as a stabilizing agent, and the CuO NP was used to prepare functional agar/CuO NP nanocomposite films using a solution casting method. The CuO NP was roughly spherical and was stable in aqueous solution. The CuO NP was homogeneously dispersed in the polymer matrix to form agar/CuO NP composite films. Incorporation of CuO NP increased the UV light barrier property with a little sacrifice of the film transparency. The mechanical properties of the films did not change significantly by the addition of CuO NP. Incorporation of CuO NP reduced the water barrier property, while increasing the surface hydrophobicity of the nanocomposite films. The agar/CuO NP nanocomposite films exhibited potent antibacterial activity against food-borne pathogens, *E. coli* and *L. monocytogenes*.

1. Introduction

Recently, research on nanocomposites composed of polymeric matrix and nanomaterials has been significantly increased due to various applications and advantages [1]. As useful nanomaterials, metal or metal oxide nanoparticles such as Ag, ZnO, and CuO nanoparticles are attracting attention due to their thermostability with various functionalities [2]. Of these nanomaterials, copper oxide nanoparticles (CuO NP) have attracted considerable attention due to the low production cost, thermal stability, comparatively lower toxicity, and strong antibacterial activity [3–6]. Various methods such as hydrothermal, precipitation, sol-gel, electrochemical, sonochemical, and green processes have been used to control the particle size, morphology, and crystallinity of CuO NP [7]. Among them, the green synthesis of CuO NP using biological materials is more advantageous than any other method because it is environmentally friendly and safe because it is low in toxicity [8]. Melanin is an interesting candidate as one of the biological materials for the green synthesis of CuO NP [9, 10]. Melanin is a multifunctional biomacromolecule that is widely distributed in the natural world with large biological functions such as light protection, antioxidation, metal ion chelating, antibacterial, anti-inflammatory, temperature regulation, free radical scavenging, and chemical protection properties [11, 12].

On the other hand, as the problem of disposal of nondegradable plastic packaging materials increases, biopolymer-based packaging materials are attracting interest as they are ecofriendly and sustainable materials with favorable structural and mechanical properties [13]. Biopolymer-based packaging materials are made using a variety of natural materials such as carbohydrates, proteins, and lipids. In particular, carbohydrate-based films exhibit good film-forming properties due to their colloidal properties with reasonable structure and mechanical properties which are highly desirable features of food packaging [14–16]. Agar, one of these carbohydrate materials, has been used to make environmentally friendly packaging films [17]. Agar is a linear polysaccharide derived from red seaweed consisting of alternating β-(1,3)- and α-(1,4)-linked galactose residues with sulfated functional groups. Agar has been widely used as a gelling agent in the food industry and has also been used to prepare transparent, flexible biopolymer films. However, relatively

weak mechanical and low water vapor barrier properties with hydrophilic nature of agar-based films restricted their application. To solve these problems, various types of nanoparticles such as nanoclays, metal or metal oxide nanomaterials, and cellulose nanocrystals are used as a reinforcing filler [1]. Substantial improvement in film properties such as mechanical, thermal, and water vapor barrier properties of biopolymer films have been reported by incorporating nanofillers into the polymer matrix [14, 18]. However, to the best of our knowledge, there is no report on the synthesis of melanin-mediated CuO NP and its reinforcement into agar to improve the structural, physical, and functional properties of bionanocomposites for food packaging applications.

Therefore, the main objectives of the present study were to synthesize CuO NP using melanin and to prepare functional agar-based nanocomposite films with improved film properties by incorporating CuO NP as a reinforcing nanofiller. The prepared CuO NP and agar/CuO NP films were characterized using various analytical methods, and their antibacterial property was evaluated.

2. Materials and Methods

2.1. Materials. As a source of melanin, food grade squid ink was purchased from Cerezo Berzosa, S.A. C/Iglesia (Carcer, Spain). Food grade agar was obtained from Gel-Tec Co. Ltd. (Seoul, Korea). Copper chloride, potassium hydroxide, and glycerol were procured from Daejung Chemicals & Metals Co., Ltd. (Siheung, Gyeonggi-do, South Korea). Brain heart infusion broth (BHI), tryptic soya broth (TSB), and bacto agar powder were purchased from Duksan Pure Chemicals Co., Ltd. (Ansan, Gyeonggi-do, South Korea). *Escherichia coli* O157: H7 ATCC 43895 and *Listeria monocytogenes* ATCC 15313 were obtained from the Korean Collection for Type Culture (KCTC, Seoul, Korea). The bacterial strains were grown in BHI and TSB agar plates and stored at 4°C before testing.

2.2. Synthesis of CuO NP. Melanin-mediated CuO NP was synthesized using copper chloride, melanin, and KOH. First, melanin was separated from the sepia ink using a centrifugal separation method, and a melanin solution of 0.1 mg/mL was prepared by dispersing the melanin precipitated in 0.1 N KOH solution [19]. Then added copper chloride (10 mM) to 100 mL of melanin solution and heated to 80°C. And 5 mM KOH solution was added dropwise to the solution until the color of the solution became dark brown, and heating was continued at 80°C for 2 h. The dark brown precipitate indicates the formation of CuO NP. CuO NP was collected by centrifugation at 10,000 rpm for 20 min, washed with distilled water until the pH became neutral, washed three times with ethanol, and dried overnight at 50°C in an oven to obtain CuO NP.

2.3. Characterization of CuO NP. The formation of CuO NP was evaluated by measuring an absorption spectrum of the solution using a UV-vis spectrophotometer (Mecasys Optizen POP Series UV/Vis, Seoul, Korea) in the range of 200-700 nm. The particle size of nanoparticles was measured by a dynamic light scattering method using a particle size analyzer (Zetasizer Nano S (ZEN 1600), Malvern Instruments Ltd., UK).

The morphological structure of CuO NP was observed using field emission scanning electron microscopy (FE-SEM, S-4800, Hitachi Co. Ltd., Matsuda, Japan), and the particle size was calculated using ImageJ (ImageJ 1.46r, National Institutes of Health, USA). The elemental analysis of CuO NP was analyzed by energy-dispersive X-ray spectroscopy (EDX) equipped with a FE-SEM microscope.

The interaction of melanin and CuO NP was evaluated using a Fourier transform infrared (FTIR) spectrophotometer (TENSOR 37 Spectrophotometer, Billerica, MA, USA). The CuO NP samples were pelletized using KBr (1 : 100 *w*/*w*), and spectra were recorded in the range of 4000-500 cm^{-1}.

X-ray diffraction patterns of CuO NP samples were recorded using an XRD diffractometer (PANalytical X'Pert PRO MRD Diffractometer, Amsterdam, Netherlands) in the range of $2\theta = 20 - 80^{\circ}$ with a scanning rate of 0.4°/min at room temperature.

2.4. Preparation of Agar/CuO NP Nanocomposite Film. Agar/CuO NP nanocomposite films were prepared using a solution casting method. For the preparation of the film-forming solution, 4 g of agar and 1.2 g of glycerol were added to 150 mL of two different concentrations of CuO NP solutions (1 and 2 wt% of agar), respectively, and mixed well at 90°C for 30 min using a magnetic stirrer. The film-forming solutions were cast on leveled Teflon film-(Cole-Parmer Instrument Co., Chicago, IL, USA) coated glass plates (24 cm × 30 cm) and allowed to dry at room temperature. After drying, films were peeled off from the plate and conditioned at 25°C and 50% RH for 48 h before the further test.

2.5. Characterizations of Agar/CuO NP Nanocomposite Film

2.5.1. Surface Morphology. Surface morphology of the nanocomposite films was tested using FE-SEM (FE-SEM, S-4800, Hitachi Co. Ltd., Matsuda, Japan) operated with an acceleration voltage of 10 kV and current of 10 μA. The samples were coated with platinum (Pt) using a vacuum sputter coater for 30 sec before the measurement. Elemental analysis of the CuO NP-incorporated agar-based composite film was analyzed by EDX with a FE-SEM microscope.

2.5.2. FTIR and XRD Analysis. Fourier transform infrared (FTIR) spectra of nanocomposite films were collected using an attenuated total reflectance-FTIR (ATR-FTIR) spectrophotometer (TENSOR 37 Spectrophotometer with OPUS 6.0 software, Billerica, MA, USA) in the range of 4000-700 cm^{-1} with a resolution of 2 cm^{-1}.

The XRD pattern of the films was analyzed using an X-ray diffractometer (PANalytical X'Pert PRO MRD diffractometer, Amsterdam, Netherlands). For this, the film samples (2.5 cm × 2.5 cm) were placed on a glass slide, and the XRD spectra were recorded using Cu Kα radiation (wavelength of 0.1541 nm) and a nickel monochromator filtering

wave at 40 kV and 30 mA. The diffraction pattern was recorded at $2\theta = 20 - 70^{\circ}$ with a scanning speed of 0.4°/min.

2.5.3. Thermal Stability. Thermogravimetric analysis (TGA) of the nanocomposite films was performed using a thermogravimetric analyzer (Hi-Res TGA 2950, TA Instruments, New Castle, DE, USA). Samples of 10 mg film were heated from 30°C to 600°C at the rate of 5°C/min. The maximum decomposition temperature at each degradation step was calculated from a derivative form of TGA (DTG) curves.

2.5.4. Surface Color and Transparency. The surface color of the film samples was evaluated using a Chroma meter (Konica Minolta, CR-400, and Tokyo, Japan). A standard white color plate ($L = 97.75$, $a = -0.49$, and $b = 1.96$) was used as a reference background for color measurements. The total color difference (ΔE) was calculated as follows:

$$\Delta E = \left[(\Delta L)^2 + (\Delta a)^2 + (\Delta b)^2\right]^{0.5}, \quad (1)$$

where ΔL, Δa, and Δb are the difference between each color values of the standard color plate and film specimen, respectively. Hunter color values (L, a, and b) were determined by taking an average of five readings from each film sample.

UV-vis spectra of nanocomposite films were recorded using a UV-vis spectrophotometer (Mecasys Optizen POP Series UV/Vis, Korea) in the wavelength range of 200-700 nm. The UV-light barrier property and transparency of the film were evaluated by measuring the light transmittance at 280 nm (T_{280}) and 660 nm (T_{660}), respectively.

2.5.5. Mechanical Properties. The thickness of the nanocomposite film was measured using a digital micrometer (Digimatic Micrometer, QuantuMike IP65, Mitutoyo, Japan) with an accuracy of 0.001 mm. An Instron Universal Testing Machine (Model 5565, Instron Engineering Corporation, Canton, MA, USA) was used to measure the tensile strength (TS), elongation at break (EB), and elastic modulus (EM) following the standard ASTM method D 882-88. For this, five rectangular strips (2.54 cm × 15 cm) from individually prepared films were cut by a precision double blade cutter (model LB.02/A, Metrotec, S.A., San Sebastian, Spain). The machine was operated in a tensile mode with a grip separation of 50 mm and a cross-head speed of 50 mm/min. The TS (MPa), EB (%), and EM (GPa) were determined using the method of Shankar et al. [9].

2.5.6. Water Vapor Permeability (WVP) and Water Contact Angle (WCA). The water vapor transmission rate (WVTR) of the nanocomposite films was performed at 25°C under 50% RH conditions using water vapor transmission measuring cups according to the ASTM E96-95 standard method [20]. Then, the WVP (g.m/m^2.Pa.s) of the film was calculated by the following equation:

$$\mathrm{WVP} = (\mathrm{WVTR} \times L)/\Delta p, \quad (2)$$

where WVTR is the measured water vapor transmission rate (g/m^2.s) through a film. L is the mean film thickness (m), and Δp is the partial water vapor pressure difference across the two sides of the film, which was calculated using the method of Gennadios et al. [20].

To determine the wetting properties, the water contact angle (CA) of the film was measured using a contact angle analyzer (Phoenix 150, Surface Electro Optics Co. Ltd., Kunpo, Korea). For the measurement, film samples were cut into rectangular pieces of 3 cm × 10 cm and placed on a black Teflon-coated steel plate using adhesive tape. Ten μL of water was dropped to the surface of the film using a syringe, and contact angle was measured on both sides of the water drop to assume symmetry and horizontal level. Five measurements were taken for each film sample, and the mean values are reported.

2.6. Antibacterial Activity. The antibacterial activity of composite films was examined against food-borne pathogenic Gram-positive bacteria, *L. monocytogenes*, and Gram-negative bacteria, *E. coli* [21]. The test bacteria were aseptically inoculated in the TSB and BHI broth, respectively, and subsequently incubated at 37°C for 15 h. The inoculum was diluted, and 200 μL of diluted inoculum (10^8-10^9 CFU/mL) was aseptically transferred to 50 mL of TSB and BHI broth containing 200 mg prepared film samples and incubated at 37°C for 12 h with mild shaking. The samples were taken out at 3, 6, 9, and 12 h of incubation, and the viable cell count was determined by diluting and plating the samples on agar plates. The broth without film was considered as a positive control. Antimicrobial tests were performed in triplicate with individually prepared films.

2.7. Statistical Analysis. The film properties were measured in triplicate with individually prepared films. For each film, three replicated measurements for surface color, optical properties, and WVP and five replicated measurements for mechanical properties and WCA were determined, and the results were provided with mean ± SD (standard deviation). One-way analysis of variance (ANOVA) was used to compare the mean differences between the samples, and the significance of each mean value was determined ($p < 0.05$) with Duncan's multiple range test of the statistical analysis system using the statistical software SPSS computer program (SPSS Inc., Chicago, IL, USA).

3. Results and Discussion

3.1. Characterization of CuO NP. The apparent color of the solution was monitored during the formation of CuO NP, and the light absorption pattern of the solution was evaluated as shown in Figure 1(a). The color of the solution becomes dark brown indicating the formation of CuO NP. Generally, the CuO NP solution exhibits a maximum optical absorption peak at ~350 nm [22, 23]. However, the maximum light absorption peak of the CuO NP solution shifted to a lower wavelength (~300 nm), suggesting a structural change in CuO NP due to the presence of melanin. The energy band gap of the synthesized CuO NP was determined using the Tauc plot [24, 25] as shown in Figure 1(b). The band gap of the CuO NP determined from the Tauc plot

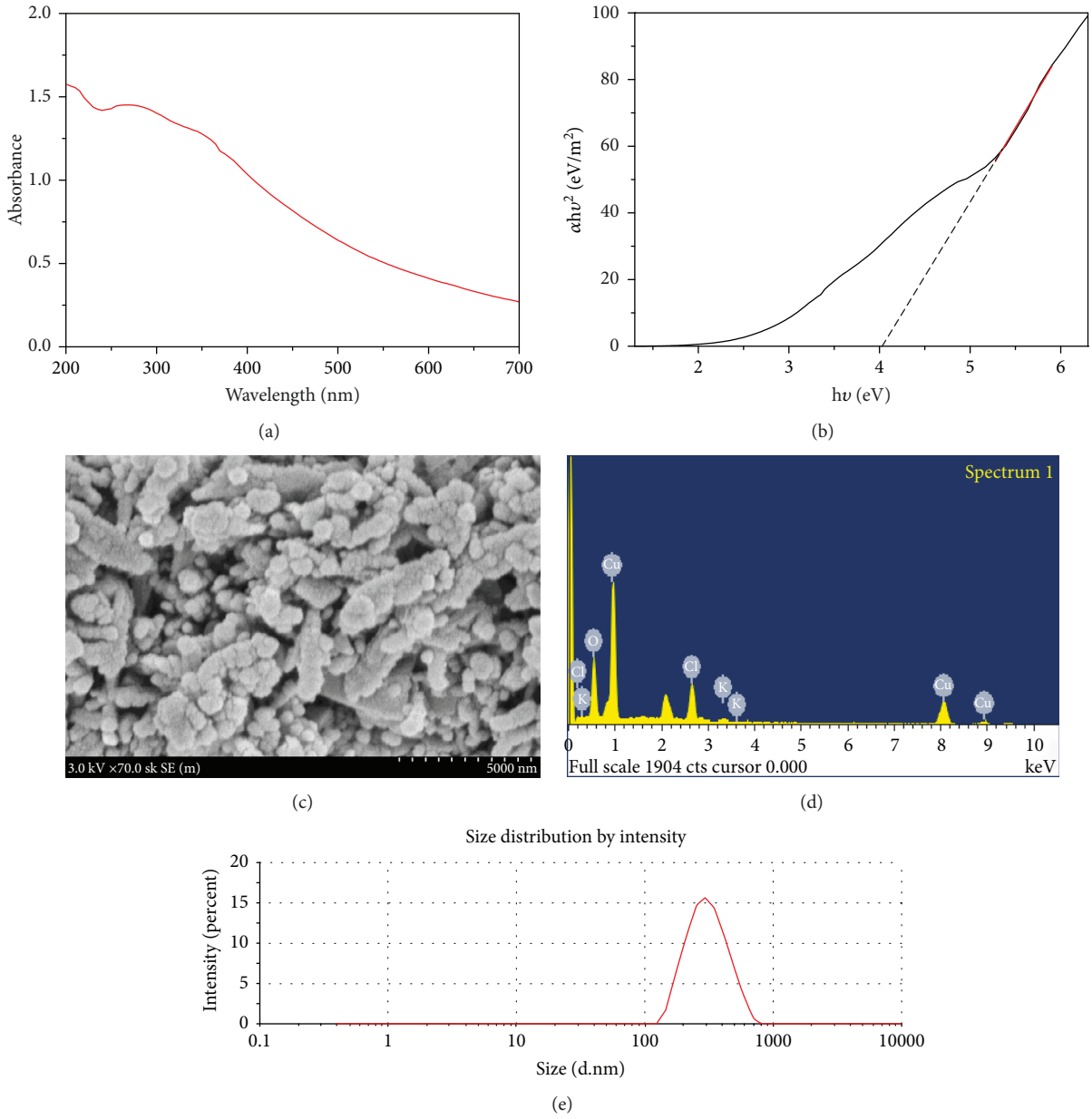

Figure 1: (a) UV-vis spectrum of melanin-mediated CuO NP, (b) Tauc plot, (c) FE-SEM images, (d) EDX spectrum, and (e) DLS spectrum of CuO NP.

was 4.01 eV, which was higher than the bulk bandgap value of CuO NP (3.5 eV) [22]. The increased band gap can be attributed to the intragap states and quantum confinement effect due to melanin [22]. The band gap obtained in this study was similar to that of CuO NP synthesized using a sonochemical method [22].

The microstructure of the synthesized CuO NP was evaluated by FE-SEM, and the resulting SEM image is shown in Figure 1(c). The CuO NP was relatively spherical in the range of 20-130 nm, and an average diameter of 66.3 ± 24 nm was estimated using ImageJ software analysis. Elemental analysis of synthesized CuO NP was performed using EDX (Figure 1(d)). The EDX spectrum showed a strong signal of Cu atoms at ~1 keV and weak signals at ~8 keV and ~9 keV, which is typical for the absorption of metallic Cu [23].

Dynamic light scattering (DLS) analysis was performed to determine the particle size and quality of the synthesized nanoparticles as shown in Figure 1(e). The hydrodynamic diameter of the synthesized CuO NP was 280.7 ± 3.8 nm, and the polydispersity index was 0.37 ± 0.02. These results show that the CuO NP prepared in this study was smaller and more monodispersed than the previously reported CuO NP [26]. The zeta potential of the CuO NP solution is -40.1 ± 2.6 mV, indicating a very stable solution. Zeta potential values above +30 mV or below -30 mV are generally considered stable due to high charge repulsion between particles sufficient to prevent aggregation and coalescence of the nanoparticles [8].

The FTIR result of CuO NP is shown in Figure 2(a). The broad absorption band at 3439 cm^{-1} was due to the -OH

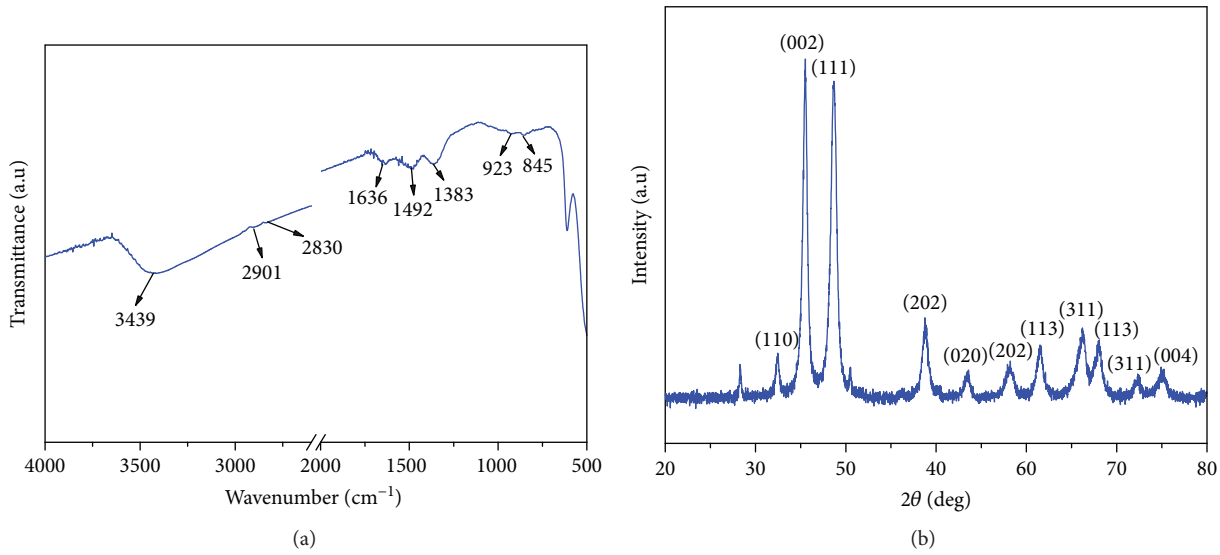

Figure 2: (a) FTIR spectrum and (b) XRD pattern of CuO NP.

group of melanin, and the broadening of the band was possibly due to the hydrogen bonding of OH groups and amine groups [27]. The peaks at 2901 and 2830 cm^{-1} were assigned to C-H stretching, and the peak observed at 1636 cm^{-1} was due to C=C stretching. The peak at 1492 cm^{-1} was due to N-H and C-N groups [28]. The peak observed at 1383 cm^{-1} was due to the bending of the O-H of carboxylic acid present in the melanin. The FTIR results showed the interaction between melanin and CuO NP during the formation of nanoparticles.

The crystalline nature of the synthesized nanoparticles evaluated using XRD analysis (Figure 2(b)). XRD reflections at $2\theta = 35.6^{\circ}$ (002) and $2\theta = 38.8^{\circ}$ (111) were ascribed to the formation of the CuO (space group $C_{2/c}$) monoclinic crystal phase [3], and the diffraction peaks of CuO corresponds to monoclinic CuO (JCPDS card 05-0661). The average crystallite size of the nanoparticles was calculated using Debye Scherer's equation ($D = 0.9\lambda/\beta \cos\theta$), and the crystallite size of CuO NP was estimated to be 13.1 nm.

3.2. Properties of Nanocomposite Film

3.2.1. Morphology. All films formed flexible films with smooth surfaces. Figure 3 shows the FE-SEM micrographs of the surface morphology of the film. Both nanocomposite films showed a uniform distribution of the nanoparticles in the polymer matrix, indicating excellent compatibility between CuO NP and agar film. The composite film with a lower concentration of CuO NP (1 wt %) showed more uniformly distributed nanoparticles than the high concentration of CuO NP (2 wt%). Similar results have been reported in agar-based films incorporated with different forms of copper nanoparticles (CuNP) [29]. Elemental analysis of the agar/-CuO NP^2 composite film showed weak signals of Cu atoms at about 1 keV and about 8 keV, which is typical for the absorption of metallic Cu, indicating the presence of CuO NP in the composite film [23]. However, the peak intensity was lower than that of CuO NP because the content of the nanoparticles in the composite film was low.

3.2.2. FTIR and XRD. FTIR spectra of the neat agar and agar/CuO NP nanocomposite films are shown in Figure 4(a). The peak at 3300 cm^{-1} observed in both films corresponded to the O-H stretching [30]. The peak at 2933 cm^{-1} was due to the C-H stretching vibration of the alkane group in the agar biopolymer chain. A typical amide I peak appeared at 1635 cm^{-1} in both films [31]. The peak at 1370 cm^{-1} corresponded to an ester sulfate group of agar. Peaks at 1040 and 930 cm^{-1} corresponded to the C=O stretching group of 3,6-anhydro-D-galactose [17]. In general, there were no notable changes in the functional groups of the nanocomposite films, suggesting that the structure of the agar was not changed by the incorporation of CuO NP. However, there was a change in the intensity of the peak due to the physical interaction between CuO NP and agar [32]. The change in intensity of FTIR peaks in agar-based composite film may be due to the van der Waals interaction between the CuO NP and the agar matrix [33]. The FTIR results also indicate good compatibility of CuO NP with biopolymers.

The crystallinity of CuO NP in the composite films was tested using the XRD analysis, and the results of XRD patterns of the agar and agar/CuO NP nanocomposite films are shown in Figure 4(b). Though the neat agar film did not show any specific diffraction peaks, the agar/CuO NP composite film exhibited characteristic diffraction peaks at 2θ of 35.45 and 38.56°, which were attributed to the (002) and (111) lattice planes of the crystalline CuO NP [10]. The observed XRD diffraction pattern of the composite film was similar to the synthesized CuO NP (Figure 2(b)), and the diffraction peaks of the resulting CuO NP are in good agreement with monoclinic CuO (JCPDS card 05-0661). Similar XRD results were also observed in agar/CuNP nanocomposite films [29].

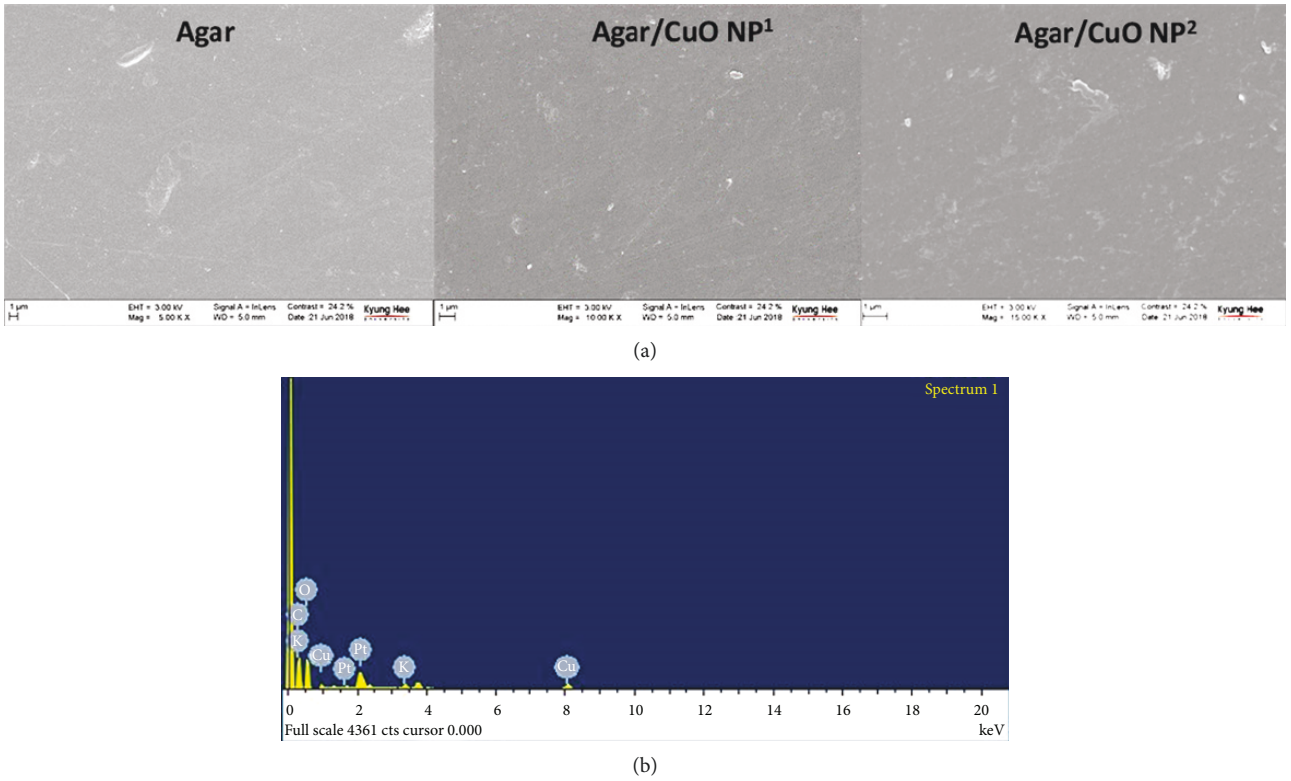

Figure 3: (a) FE-SEM micrographs and (b) EDX spectrum of agar/CuO NP nanocomposite films.

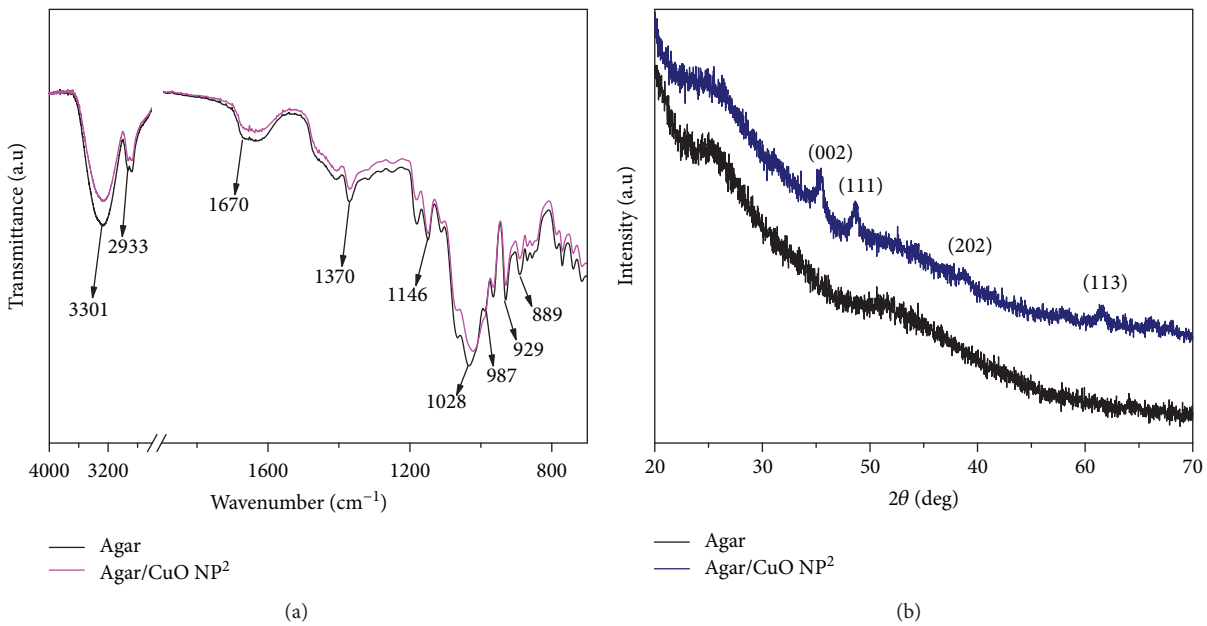

Figure 4: (a) FTIR spectra and (b) XRD patterns of agar/CuO NP nanocomposite film.

3.2.3. Thermal Stability. TGA and DTG of agar and agar/-CuO NP nanocomposite films are shown in Figure 5. The TGA thermogram shows the weight loss pattern of the film due to thermal decomposition, and the DTG curve provides information on the maximum decomposition temperature at each step of thermal decomposition. Both neat agar and agar/CuO NP nanocomposite films exhibited three stages of thermal decomposition. The first weight loss was observed at 90°C and 95°C, respectively, for the neat agar and agar/-CuO NP nanocomposite films due to moisture evaporation from the film. The second decomposition started at about 200°C and reached a maximum of 250°C, which was due to the glycerol decomposition used as a plasticizer [29]. The main thermal degradation occurred at about 300°C due to

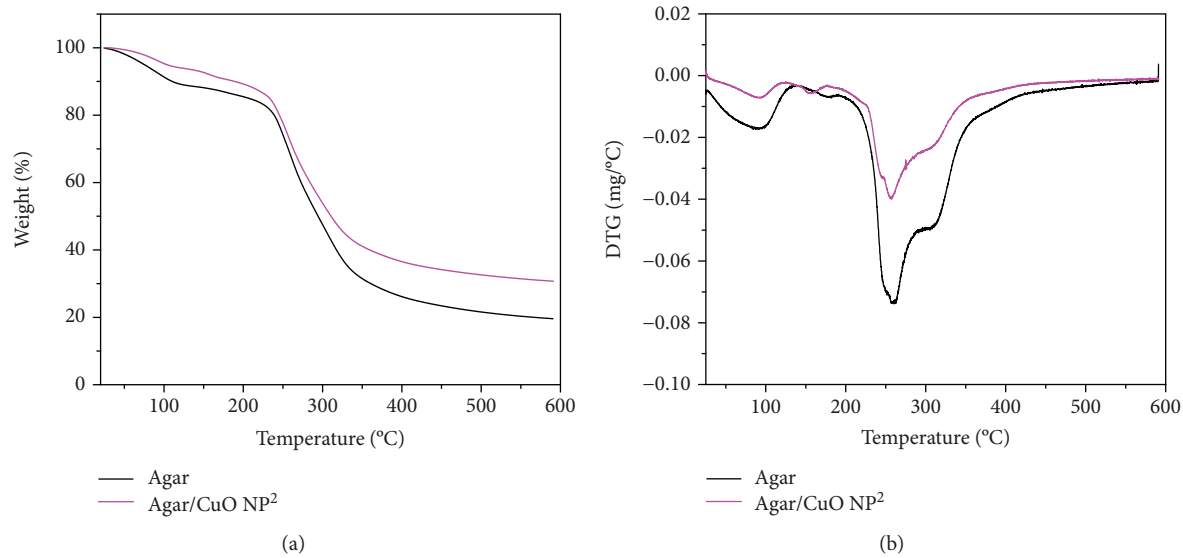

Figure 5: TGA and DTG thermograms of agar/CuO NP nanocomposite film.

Table 1: Surface color and transmittance of agar-based films.

Films	L	a	b	ΔE	T_{280} (%)	T_{660} (%)
Agar	90.6 ± 0.3^{c}	-0.64 ± 0.1^{a}	7.3 ± 0.1^{a}	3.2 ± 0.2^{a}	44.5 ± 2.5^{c}	88.5 ± 0.9^{c}
Agar/CuO NP[1]	60.3 ± 0.4^{b}	6.92 ± 0.1^{b}	20.3 ± 0.1^{b}	36.4 ± 0.3^{b}	9.9 ± 1.9^{b}	49.7 ± 0.1^{b}
Agar/CuO NP[2]	42.4 ± 1.3^{a}	10.24 ± 0.1^{c}	19.04 ± 0.2^{b}	53.0 ± 1.2^{c}	1.4 ± 1.2^{a}	26.9 ± 0.1^{a}

The values are represented as mean ± standard deviation. The value in the same column followed by the same letter is not significantly ($p > 0.05$) different.

the polymeric degradation of agar [29]. The second and third stages of maximal degeneration of the agar/CuO NP nanocomposite film were slightly lower than those of the neat agar film. The char residues of the neat agar and agar/CuO NP nanocomposite films at 600°C were 19.6% and 30.6%, respectively. The somewhat higher char content of the agar-based films was probably due to the nonignitable minerals of the agar, and the more char residues of the agar/CuO NP nanocomposite film was mainly due to the presence of heat-resistant nanoparticles in the film [17]. Similar thermal degradation patterns were observed when different types of CuNP were incorporated into agar-based films [29].

3.2.4. Surface Color and Transmittance. The surface color of the neat agar and agar/CuO NP nanocomposite films determined using Hunter L, a, and b values is shown in Table 1. All color values of agar-based films changed significantly ($p < 0.05$) by the incorporation of CuO NP. Especially, the lightness (Hunter L value) of the film decreased profoundly depending on the concentration of CuO NP. The redness (Hunter a value) and yellowness (Hunter b value) increased, and consequently, the overall color difference (ΔE) of the agar film increased by the incorporation of CuO NP.

The UV-barrier property and transparency of the film are described in Table 1. The light transmittance values of the film at 280 nm and 660 nm to evaluate the UV-barrier property and transparency of the films, respectively, are shown in Table 1. The neat agar film was highly transparent with T_{660} of 88.5%, and it became translucent with less than 50% of T_{660} after incorporation of CuO NP, but it was still able to see through. Ultraviolet transmission of the agar/-CuO NP composite film was blocked more than visible light. When 2 wt% of CuO NP was incorporated into the agar film, UV light was almost completely blocked at 400 nm or less. The high UV blocking properties of agar/CuO NP nanocomposite films may be due to the presence of melanin and CuO NP. Shankar et al. also observed an increased UV-barrier property in agar/CuNP composite films [29]. The agar/CuO NP composite films, which have increased UV-barrier properties with somewhat sacrificing transparency, can be used as a UV barrier food packaging material to prevent degradation of packaged food due to a photochemical reaction.

3.2.5. Mechanical Properties. The mechanical properties of the nanocomposite films are represented in Table 2. The thickness of agar/CuO NP composite films increased significantly ($p < 0.05$) than that of the neat agar film, which was due to an increase in the solid content [34]. The mechanical strength (TS) and flexibility (EB) of the agar/CuO NP composite films did not change significantly ($p > 0.05$) after incorporation of CuO NP, but the stiffness (EM) of the composite film was decreased slightly compared to the neat agar film. These results are in good agreement with those of agar/CuNP composite films [29]. The TS and other

Table 2: Mechanical properties, water vapor permeability, and water contact angle of agar-based films.

Films	Thickness (μm)	TS (MPa)	EB (%)	EM (GPa)	WVP ($\times 10^{-9}$ g.m/m^2.Pa.s)	WCA (deg.)
Agar	49.0 ± 0.4^a	45.1 ± 0.6^a	4.4 ± 0.6^a	2.17 ± 0.05^b	2.99 ± 0.3^a	40.9 ± 3.8^a
Agar/CuO NP^1	59.2 ± 0.6^c	45.1 ± 1.8^a	4.8 ± 0.6^a	1.85 ± 0.10^a	3.99 ± 0.4^b	50.2 ± 4.0^b
Agar/CuO NP^2	55.5 ± 0.7^b	44.9 ± 0.9^a	4.7 ± 0.3^a	1.95 ± 0.10^{ab}	4.35 ± 0.5^b	51.2 ± 2.7^b

The values are represented as mean ± standard deviation. The value in the same column followed by the same letter is not significantly ($p > 0.05$) different.

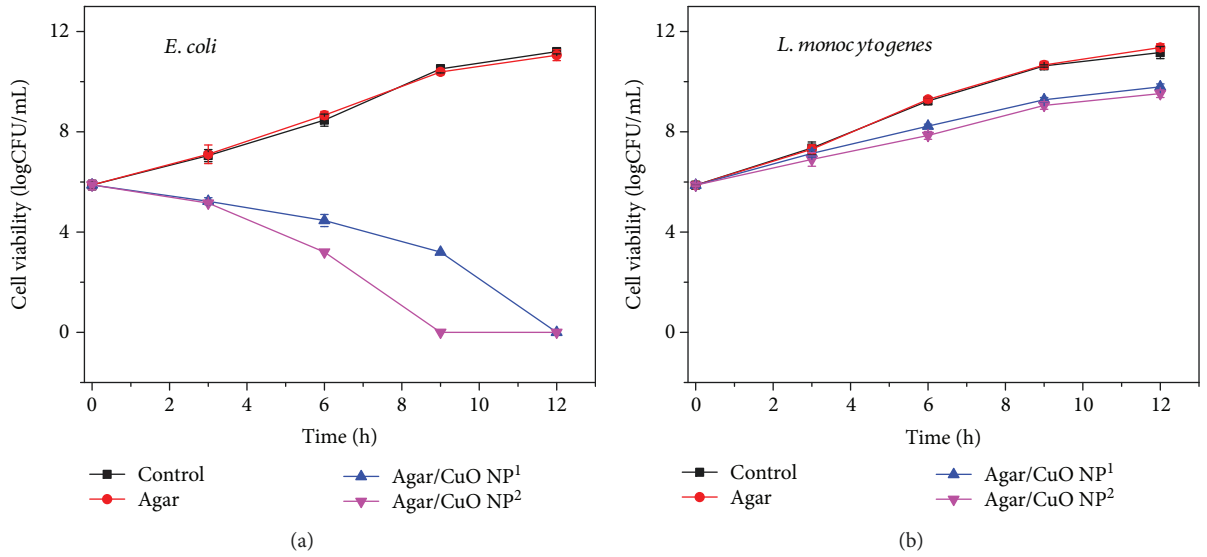

Figure 6: Antimicrobial activity of agar/CuO NP nanocomposite films against *E. coli* and *L. monocytogenes*.

mechanical properties of the films are primarily dependent on the distribution of the inter- and intramolecular interaction between polymer chains [35].

3.2.6. Water Vapor Permeability (WVP) and Water Contact Angle (WCA). The WVP and WCA of agar and agar/CuO NP composite films are also shown in Table 2. The WVP of the agar/CuO NP composite films was significantly higher than that of the neat agar film, indicating that the water vapor barrier of the composite films decreased compared to the neat agar film. The increased WVP of the nanocomposite film may be due to the formation of a discontinuous phase between nanoparticles and agar matrix resulting in a porous structure in the film [34].

The surface hydrophobicity of the nanocomposite film was evaluated by measuring the water contact angle as shown in Table 2. WCA of the biopolymer film is commonly used to determine the surface hydrophobicity or hydrophilicity of the film [36]. Biopolymer films with WCA greater than 65° are considered to have a hydrophobic surface [37]. The CA of the neat agar film was $40.9 \pm 3.8°$, and it increased significantly to $50.2 \pm 4.0°$ and $51.2 \pm 2.7°$ when 1 and 2 wt% of CuO NP was incorporated. The increase in the WCA can be due to the relatively more hydrophobic nature of CuO NP than that of agar. Similarly, the hydrophobicity of agar films increased when CuNP was incorporated into the agar film [29].

3.3. Antibacterial Activity. The antimicrobial activity of the neat agar and agar/CuO NP nanocomposite films was tested against food-borne pathogenic bacteria, *E. coli* and *L. monocytogenes*, and the results are shown in Figure 6. As expected, the neat agar film did not exhibit any antibacterial activity, but CuO NP-incorporated nanocomposite films exhibited significant antibacterial activity depending on the types of bacteria tested and the concentration of CuO NP. As shown in Figure 6, the agar/CuO NP composite films exhibited strong antibacterial activity against *E. coli*; that is, the bacterial count steadily decreased after contacting with the nanocomposite films and the growth of the bacteria completely stopped after 9 h and 12 h of culture, respectively, with 2 wt% and 1 wt% of CuO NP-incorporated agar films. On the other hand, the agar/CuO NP composite film exhibited only a small amount of antimicrobial activity against *L. monocytogenes* and only decreased the proliferation rate of the test bacteria. Differences in the antibacterial activity of CuO NP against Gram-positive and Gram-negative bacteria are mainly due to differences in the cell wall structure of the test microorganisms. Gram-positive bacteria consist of a thick cell wall structure with multiple layers of peptidoglycan, and gram-negative bacteria consist of a complex cell wall structure consisting of a thin peptidoglycan layer surrounded by an outer cell membrane [32, 38]. The lower antibacterial activity of CuO NP against *L. monocytogenes* may be due to the difficulty of CuO NP transferring to the

cytoplasm through the thick cell walls [16, 38]. The mechanism of inhibition of bacterial growth by CuO NP is not yet clearly elucidated, but it is believed that copper ions are released in water to interact with negatively charged cell membrane proteins to destroy cell walls and cause cell death [39]. It has also been suggested that CuO NP can interact with DNA to inhibit the regeneration of bacterial cells [23]. CuO NP also may result in the production of free radicals, reactive oxygen species, and lipid and protein oxidation, leading to bacterial cell death [40].

4. Conclusions

Spherical CuO NP was prepared using melanin as a stabilizing agent, and the CuO NP was used to prepare functional agar-based nanocomposite films. The FE-SEM micrograph confirmed that the CuO NP was uniformly dispersed in the agar matrix, and FTIR confirmed that the CuO NP stabilized with melanin was compatible with the agar polymer matrix. The agar/CuO NP nanocomposite film exhibited excellent UV barrier property. Mechanical properties of the nanocomposite film were maintained as the same level as the neat agar film, and the hydrophobicity of the nanocomposite film increased while water barrier property and thermal stability decreased compared to the neat agar film. The agar/CuO NP nanocomposite films exhibited a distinctive antibacterial activity against *E. coli* and *L. monocytogenes*, but the antibacterial activity was more pronounced against *E. coli*. The agar/CuO NP nanocomposite films with a strong UV barrier and antibacterial properties have a high potential as environmentally friendly functional food packaging films.

Data Availability

The data used to support the findings of this study are included within the article.

Conflicts of Interest

The authors declare that they have no conflicts of interest.

Acknowledgments

This work was supported by the Korea Institute of Planning and Evaluation for Technology in Food, Agriculture, Forestry (IPET) through the High Value-added Food Technology Development Program funded by Ministry of Agriculture, Food and Rural Affairs (MAFRA) (20171048), Republic of Korea.

References

[1] J.-W. Rhim, H.-M. Park, and C.-S. Ha, "Bio-nanocomposites for food packaging applications," *Progress in Polymer Science*, vol. 38, no. 10-11, pp. 1629–1652, 2013.

[2] P. Gong, H. Li, X. He et al., "Preparation and antibacterial activity of Fe_3O_4@Ag nanoparticles," *Nanotechnology*, vol. 18, no. 28, p. 285604, 2007.

[3] Y. Haldorai and J.-J. Shim, "Multifunctional chitosan-copper oxide hybrid material: photocatalytic and antibacterial activities," *International Journal of Photoenergy*, vol. 2013, Article ID 245646, 8 pages, 2013.

[4] P. S. Kumar, M. Selvakumar, S. G. Babu, S. K. Jaganathan, S. Karuthapandian, and S. Chattopadhyay, "Novel CuO/chitosan nanocomposite thin film: facile hand-picking recoverable, efficient and reusable heterogeneous photocatalyst," *RSC Advances*, vol. 5, no. 71, pp. 57493–57501, 2015.

[5] A. M. El Sayed, S. El-Gamal, W. M. Morsi, and G. Mohammed, "Effect of PVA and copper oxide nanoparticles on the structural, optical, and electrical properties of carboxymethyl cellulose films," *Journal of Materials Science*, vol. 50, no. 13, pp. 4717–4728, 2015.

[6] M. Safaei and M. Taran, "Optimized synthesis, characterization, and antibacterial activity of an alginate–cupric oxide bionanocomposite," *Journal of Applied Polymer Science*, vol. 135, no. 2, article 45682, 2018.

[7] M. E. Grigore, E. R. Biscu, A. M. Holban, M. C. Gestal, and A. M. Grumezescu, "Methods of synthesis, properties and biomedical applications of CuO nanoparticles," *Pharmaceuticals*, vol. 9, no. 4, p. 75, 2016.

[8] S. Roy, T. K. Das, G. P. Maiti, and U. Basu, "Microbial biosynthesis of nontoxic gold nanoparticles," *Materials Science and Engineering B*, vol. 203, pp. 41–51, 2016.

[9] S. Shankar, L.-F. Wang, and J.-W. Rhim, "Preparation and properties of carbohydrate-based composite films incorporated with CuO nanoparticles," *Carbohydrate Polymers*, vol. 169, pp. 264–271, 2017.

[10] M. Apte, G. Girme, R. Nair, A. Bankar, A. Ravi Kumar, and S. Zinjarde, "Melanin mediated synthesis of gold nanoparticles by *Yarrowia lipolytica*," *Materials Letters*, vol. 95, pp. 149–152, 2013.

[11] K. Shanmuganathan, J. H. Cho, P. Iyer, S. Baranowitz, and C. J. Ellison, "Thermooxidative stabilization of polymers using natural and synthetic melanins," *Macromolecules*, vol. 44, no. 24, pp. 9499–9507, 2011.

[12] Y. Liu and J. D. Simon, "Isolation and biophysical studies of natural eumelanins: applications of imaging technologies and ultrafast spectroscopy," *Pigment Cell Research*, vol. 16, no. 6, pp. 606–618, 2003.

[13] V. D. Alves, R. Castelló, A. R. Ferreira, N. Costa, I. M. Fonseca, and I. M. Coelhoso, "Barrier properties of carrageenan/pectin biodegradable composite films," *Procedia Food Science*, vol. 1, pp. 240–245, 2011.

[14] P. Kanmani and J.-W. Rhim, "Properties and characterization of bionanocomposite films prepared with various biopolymers and ZnO nanoparticles," *Carbohydrate Polymers*, vol. 106, pp. 190–199, 2014.

[15] M. Atef, M. Rezaei, and R. Behrooz, "Preparation and characterization agar-based nanocomposite film reinforced by nanocrystalline cellulose," *International Journal of Biological Macromolecules*, vol. 70, pp. 537–544, 2014.

[16] Y. Shchipunov, "Bionanocomposites: green sustainable materials for the near future," *Pure and Applied Chemistry*, vol. 84, no. 12, pp. 2579–2607, 2012.

[17] S. Shankar and J. W. Rhim, "Amino acid mediated synthesis of silver nanoparticles and preparation of antimicrobial agar/silver nanoparticles composite films," *Carbohydrate Polymers*, vol. 130, pp. 353–363, 2015.

[18] S. M. Liff, N. Kumar, and G. H. McKinley, "High-performance elastomeric nanocomposites via solvent-exchange processing," *Nature Materials*, vol. 6, no. 1, pp. 76–83, 2007.

[19] Y. Wang, T. Li, X. Wang et al., *Biomacromolecules*, vol. 17, no. 11, pp. 3782–3789, 2016.

[20] A. Gennadios, C. L. Weller, and C. H. Gooding, "Measurement errors in water vapor permeability of highly permeable, hydrophilic edible films," *Journal of Food Engineering*, vol. 21, no. 4, pp. 395–409, 1994.

[21] A. A. Oun and J.-W. Rhim, "Carrageenan-based hydrogels and films: effect of ZnO and CuO nanoparticles on the physical, mechanical, and antimicrobial properties," *Food Hydrocolloids*, vol. 67, pp. 45–53, 2017.

[22] N. R. Dhineshbabu, V. Rajendran, N. Nithyavathy, and R. Vetumperumal, "Study of structural and optical properties of cupric oxide nanoparticles," *Applied Nanoscience*, vol. 6, no. 6, pp. 933–939, 2016.

[23] M. S. Jadhav, S. Kulkarni, P. Raikar, D. A. Barretto, S. K. Vootla, and U. S. Raikar, "Green biosynthesis of CuO & Ag–CuO nanoparticles from *Malus domestica* leaf extract and evaluation of antibacterial, antioxidant and DNA cleavage activities," *New Journal of Chemistry*, vol. 42, no. 1, pp. 204–213, 2017.

[24] S. Roy, S. Mishra, P. Yogi, S. K. Saxena, P. R. Sagdeo, and R. Kumar, "Synthesis of conducting polypyrrole-titanium oxide nanocomposite: study of structural, optical and electrical properties," *Journal of Inorganic and Organometallic Polymers and Materials*, vol. 27, Supplement 1, pp. 257–263, 2017.

[25] J. Tauc, R. Grigorovici, and A. Vancu, "Optical properties and electronic structure of amorphous germanium," *Physica Status Solidi B: Basic Solid State Physics*, vol. 15, no. 2, pp. 627–637, 1966.

[26] S. Saif, A. Tahir, T. Asim, and Y. Chen, "Plant mediated green synthesis of CuO nanoparticles: comparison of toxicity of engineered and plant mediated CuO nanoparticles towards *Daphnia magna*," *Nanomaterials*, vol. 6, no. 11, p. 205, 2016.

[27] Y. Wang, T. Li, P. Ma et al., "Simultaneous enhancements of UV-shielding properties and photostability of poly(vinyl alcohol) via incorporation of sepia eumelanin," *ACS Sustainable Chemistry & Engineering*, vol. 4, no. 4, pp. 2252–2258, 2016.

[28] M. L. Roldán, S. A. Centeno, and A. Rizzo, "An improved methodology for the characterization and identification of sepia in works of art by normal Raman and SERS, complemented by FTIR, Py-GC/MS, and XRF," *Journal of Raman Specroscopy*, vol. 45, no. 11-12, pp. 1160–1171, 2014.

[29] S. Shankar, X. Teng, and J.-W. Rhim, "Properties and characterization of agar/CuNP bionanocomposite films prepared with different copper salts and reducing agents," *Carbohydrate Polymers*, vol. 114, pp. 484–492, 2014.

[30] J.-W. Rhim, L.-F. Wang, Y. Lee, and S.-I. Hong, "Preparation and characterization of bio-nanocomposite films of agar and silver nanoparticles: laser ablation method," *Carbohydrate Polymers*, vol. 103, pp. 456–465, 2014.

[31] S. Ghosh, R. Kaushik, K. Nagalakshmi et al., "Antimicrobial activity of highly stable silver nanoparticles embedded in agar-agar matrix as a thin film," *Carbohydrate Research*, vol. 345, no. 15, pp. 2220–2227, 2010.

[32] S. Anitha, B. Brabu, D. J. Thiruvadigal, C. Gopalakrishnan, and T. S. Natarajan, "Optical, bactericidal and water repellent properties of electrospun nano-composite membranes of cellulose acetate and ZnO," *Carbohydrate Polymers*, vol. 87, no. 2, pp. 1065–1072, 2012.

[33] S. Roy, S. Shankar, and J.-W. Rhim, "Melanin-mediated synthesis of silver nanoparticle and its use for the preparation of carrageenan-based antibacterial films," *Food Hydrocolloids*, vol. 88, pp. 237–246, 2019.

[34] S. Shankar, X. Teng, G. Li, and J.-W. Rhim, "Preparation, characterization, and antimicrobial activity of gelatin/ZnO nanocomposite films," *Food Hydrocolloids*, vol. 45, pp. 264–271, 2015.

[35] H. Chambi and C. Grosso, "Edible films produced with gelatin and casein cross-linked with transglutaminase," *Food Research International*, vol. 39, no. 4, pp. 458–466, 2006.

[36] J.-F. Su, Z. Huang, X.-Y. Yuan, X.-Y. Wang, and M. Li, "Structure and properties of carboxymethyl cellulose/soy protein isolate blend edible films crosslinked by Maillard reactions," *Carbohydrate Polymers*, vol. 79, no. 1, pp. 145–153, 2010.

[37] E. A. Vogler, "Structure and reactivity of water at biomaterial surfaces," *Advances in Colloid and Interface Science*, vol. 74, no. 1-3, pp. 69–117, 1998.

[38] S. Pal, Y. K. Tak, and J. M. Song, "Does the antibacterial activity of silver nanoparticles depend on the shape of the nanoparticle? A study of the gram-negative bacterium *Escherichia coli*," *Applied and Environmental Microbiology*, vol. 73, no. 6, pp. 1712–1720, 2007.

[39] Z. M. Sui, X. Chen, L. Y. Wang et al., "Capping effect of CTAB on positively charged Ag nanoparticles," *Physica E: Low-dimensional Systems and Nanostructures*, vol. 33, no. 2, pp. 308–314, 2006.

[40] A. K. Chatterjee, R. Chakraborty, and T. Basu, "Mechanism of antibacterial activity of copper nanoparticles," *Nanotechnology*, vol. 25, no. 13, p. 135101, 2014.